Quantifying Proprioceptive Reflexes During Position Control of the Human Arm

Alfred C. Schouten*, Erwin de Vlugt, J. J. (Bob) van Hilten, and Frans C. T. van der Helm

***Abstract*—This study aimed to analyse the dynamic properties of the muscle spindle feedback system of shoulder muscles during a posture task. External continuous force disturbances were applied at the hand while subjects had to minimize their hand displacements. The results were analysed using two frequency response functions (FRFs) from which the model parameters were derived, being 1) the mechanical admittance and 2) the reflexive impedance. These FRFs were analysed by a neuromusculoskeletal model that implicitly separates the reflexive feedback properties (position, velocity and acceleration feedback gains) from intrinsic muscle visco-elasticity. The results show substantial changes in estimated reflex gains under conditions of variable bandwidth of the applied force disturbance or variable degrees of external damping. Position and velocity feedback gains were relatively larger when the force disturbance contained only low frequencies. With increasing damping of the environment, acceleration feedback gain decreased, velocity feedback gain remained almost constant and position feedback gain increased. It is concluded that under the aforementioned circumstances, the reflex system increases its gains to maximize the mechanical resistance to external force disturbances while preserving sufficient stability.**

***Index Terms*—Arm admittance, electromyography, identification, proprioceptive reflexes, reflexive impedance.**

I. Introduction

STUDIES addressing the role of proprioceptive reflexes in the regulation of movement and posture have been informative in understanding the impact of diseases with abnormal muscle tone including spasticity, dystonia or Parkinson's disease [1]–[3]. Studies on the role of proprioceptive reflexes in the regulation of muscle tone have mainly applied an investigation based on signal properties, such as EMG amplitude and onset delays [4]–[7]. From these studies important features of the proprioceptive reflex system emerged showing the influence of position and force tasks on proprioceptive reflex magnitude. However these studies have not provided insight into the functional contribution of proprioceptive reflexes, i.e., to the dynamic relation between force and position (mechanical admittance), which is crucial in the understanding of how reflexes contribute to movement and posture. Few studies have focused on the role of proprioceptive reflexes on the overall mechanical behavior of joints [8]–[10]. These studies have used quantification methods that basically rely on specific neuromuscular models and optimisation algorithms to minimize the difference between measured and predicted variables. Hitherto, all studies have used an indirect approach by estimating reflex gains from the mechanical admittance. In the mechanical response, intrinsic muscle visco-elasticity and reflexive contributions coexist. Therefore, assumptions on the reflexive component were necessary to separate the intrinsic and reflexive contributions. Such assumptions on reflex behaviour may introduce a bias in the model parameters. Consequently, there is a need for methods that use a more direct way of reflex quantification.

In a recent study [11], a method was introduced to simultaneously estimate the frequency response functions of the mechanical admittance and the reflexive impedance. The reflexive impedance describes the dynamic relation between recorded hand position and muscle activation, as measured by surface EMG activity. The goal of the present study is to identify reflex behavior under different loading conditions in case of a funcional position task using both the mechanical admittance and the reflexive impedance. Proprioceptive reflexes in the human arm are quantified under conditions of variable bandwidth of the applied force disturbance or variable degrees of external damping. Consistent parameter estimates were obtained. In general, reflex gains were attenuated when the bandwidth of the external force disturbance increased towards the eigenfrequency of the arm. Furthermore increased external damping enlarged the reflex gains. Functional implications of these results are discussed. This study showed that detailed properties of the neuromuscular control system can be quantified by incorporating EMG in the mechanical analysis. This methodology opens new possibilities to further investigate the role of proprioceptive reflexes during human motor control, for instance the modulation of reflex gain while interacting with different environments.

II. Material and Methods

A. Subjects

Two experiments were carried out. In the main experiment ten healthy subjects (four women, three left handed) participated with a mean (SD) age of 25.8 (7.0) years. In a second experiment, to estimate the muscle activation dynamics, five subjects (two women, two left handed) participated with a mean (SD) age of 25.4 (3.2) years. All subjects gave informed consent prior to the experiment. All experiments were conducted on the right arm.

Manuscript received October 25, 2006; revised April 7, 2007. *Asterisk indicates corresponding author.*

*A. C. Schouten is with the Department of Biomechanical Engineering, Delft University of Technology, Mekelweg 2, 2628 CD Delft, The Netherlands (e-mail: a.c.schouten@tudelft.nl).

E. de Vlugt and F. C. T. van der Helm are with the Department of Biomechanical Engineering, Delft University of Technology, 2628 CD Delft, The Netherlands.

J. J. van Hilten is with the Department of Neurology, Leiden University Medical Center, Leiden 2333 ZA, The Netherlands.

Digital Object Identifier 10.1109/TBME.2007.899298

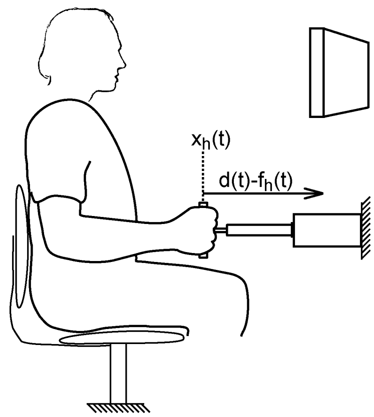

Fig. 1. Experimental setup. The subject sits on a chair and holds the handle with the right hand. The piston can move forwards and backwards. The hand force, $f_h(t)$, applied to the hydraulic manipulator is measured by a force transducer mounted between the handle and the piston. The manipulator controls the position of the handle, $x_h(t)$ and is based on the sum of the hand force, external force disturbance, $d(t)$, and the simulated virtual dynamics (environment).

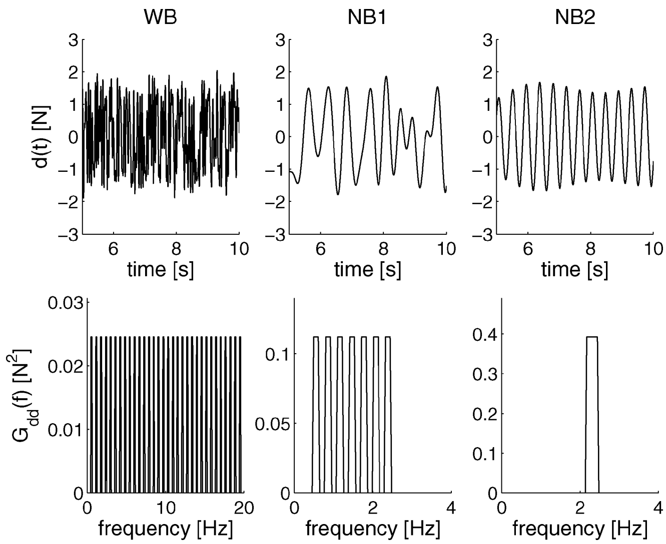

Fig. 2. Examples of disturbance signals. Left: WB; middle: NB1 $f_h = 2.4$ Hz; right: NB2 $f_c = 2.3$ Hz. Upper plots: 5-s fragment of the signals; lower plots: power spectral densities of the signals. For clarity the signals are scaled to a root mean square (RMS) value of one. Each peak in the power spectral densities represents a cluster of four (WB, NB1) or eight (NB2) adjacent frequencies.

B. Apparatus

Force disturbances were applied to the hand by means of a linear manipulator, see Fig. 1. The manipulator is described in detail previously [10], [12]. The subject was able to move the handle of the manipulator for- and backwards, resulting in ante-/retroflexion of the gleno-humeral joint. The manipulator "felt" like a mass-spring-damper system to the subject and the parameters of this (virtual) environment are adjustable. In this study the mass, m_e, was set to a fixed value of 1 kg. The damping, b_e, was varied between the trials, see Procedures. No virtual spring was used ($k_e = 0$ N/m).

C. Procedures

1) Main Experiment: In the main experiment subjects had to hold the handle and were instructed to *"minimize the displacements"* of the handle, while continuous random force disturbances were applied for 30 seconds (task *stiff*). The actual position of the handle was shown on a display to assist the subjects and to prevent drift. Only a few trials were necessary to get the subject acquainted with the task. The following experimental conditions were applied:

- Wide bandwidth disturbance without external damping (WB *stiff*). The WB disturbance signal had power between between 0.5 and 20 Hz. This condition is referred to as the reference condition.
- WB disturbance without external damping and the task *slack* (WB *slack*). Here the task instruction was different from the other: the subject was asked to relax his/her arm muscles and not to react to the disturbance. This task was only used to improve to estimate of the arm mass.
- WB disturbance with external damping. The damping was assigned values of 50, 100, 150, 200 Ns/m (B50, B100, B150, B200). These and the following tasks were used to provoke different proprioceptive reflex gains.
- Narrow bandwidth disturbance type 1 (NB1) without external damping. The disturbance signals had a variable bandwidth; the lowest frequency was fixed at 0.5 Hz and the highest frequency f_h varied between 1.2 and 3.7 Hz (1.2, 1.5, 1.8, 2.4, 3.1, 3.7 Hz).
- Narrow bandwidth disturbance type 2 (NB2) without external damping. The signals had a bandwidth of 0.3 Hz concentrated around a variable center frequency, f_c, of 1.3 up to 7 Hz (1.3, 1.8, 2.3, 3, 4, 5, 6, 7 Hz).

The twenty different conditions were repeated four times, resulting in eighty trials of 30 seconds each. The trials were presented in a random order. In between the trials the subject could rest as long as he/she wanted to prevent fatigue. All disturbance signals were designed in the frequency domain as so-called multisine signals with optimized crest factor [11], [13], [14]. Because multisine signals are deterministic, no bias or variance were introduced in the estimated spectral densities [14], [15].

To improve the signal-to-noise ratio (SNR) of the EMG and to allow reliable identification of the reflexive impedance, the power of the disturbance signal was distributed over a limited number of frequencies within the bandwidth. For the WB disturbance the signal power was uniformly distributed over 32 equidistantly spaced clusters of four adjacent frequencies, i.e., 25% of the frequencies within the bandwidth are excited [11]. The data analysis required clusters of four adjacent frequencies for averaging. For the NB1 disturbances 50% of the frequencies within the bandwidth were excited, and consequently each NB1 signal contained a different number of clusters (ranging from three clusters for $f_h = 1.2$ Hz up to 11 clusters for $f_h = 3.7$ Hz). For the NB2 disturbances the power was distributed in one cluster of eight adjacent frequencies. Fig. 2 shows examples of the disturbance signals, the lower plots show the power spectral densities of the signals.

To justify the use of linear model approximations the position deviations must be kept small within each condition. Prior to the trials each condition was tested and the amplitude of the force disturbance was adjusted for each condition to obtain a root-mean-square (RMS) value for the position of approximately 3 mm.

Since recorded EMG is an electric signal which is meaningless to the mechanical properties, the EMG to force ratio was determined to obtain a relative measure of the muscle force. Therefore, subjects were required to perform isometric push and pull tasks, prior to and after the main experiment. The subjects had to maintain constant force levels for 10 s (-25, -20, -15, 0, 15, 20, 25 N) by pushing or pulling against the handle, which was controlled to be in a fixed (rigid) position. During these isometric trials the reference force together with the actual force at the handle were shown on the display to assist the subject in performing the task. The EMG to force ratio was determined by linear regression.

2) Activation Dynamics Experiment: The EMG to force ratio provides the static relation between muscle activation and muscle force. The dynamic relation between muscle activation and muscle force was determined in a secondary isometric experiment. The secondary experiment started and ended with the same isometric push/pull tasks as the main experiment. The experiment consisted of eight trials of 30 s. During these trials the subjects performed isometric tasks and were asked to make block-shaped forces between approximately 25 N push and pull.

D. Data Processing

1) Signal Recording and Processing: During a trial the force disturbance $d(t)$, the position of the handle $x_h(t)$, the force at the handle $f_h(t)$, and the EMG of four relevant shoulder muscles (e_1: m. pectoralis major, e_2: m. deltoideus anterior, e_3: m. deltoideus posterior, and e_4: m. latissimus dorsi) were recorded at 2500-Hz sample frequency with a 16-bit resolution. Before recording, the EMG signals were highpass filtered to remove DC components and movement artefacts (20 Hz, third-order Butterworth), and lowpass filtered to prevent aliasing (1 kHz, third-order Butterworth). This study investigates stationary behavior and to remove any initial transient effect the first 9464 samples ($\approx$ 4 s) from each recording were eliminated, leaving 2^{16} samples ($\approx$ 26 s) for further processing.

The EMG signals were used 1) to estimate the amount of co-activation expressed by the mean EMG and 2) to construct the muscle activation $a(t)$. The procedure of EMG treatment is described previously in [11] and will be briefly summarized. To improve the quality of the EMG signals a prewhitening filter is implemented, following the procedures as described in [16]. The power spectral densities of the EMGs during the maximum isometric push and pull tasks (25 N) are used to obtain the parameters of the prewhitening filter (sixth order).

For small variations in muscle co-activation it reasonable to assume that the intrinsic muscle visco-elasticity linearly scale with the co-activation level [17]. Therefore, mean EMG, u_0, was determined as a measure for muscle co-activation. To calculate the mean EMG the integrated rectified EMG, IEMG, of each muscle during a trial was calculated

$$\mathrm{IEMG}_i = \frac{1}{n}\sum_{k=1}^{n} |e_{w,i}(t_k)| \tag{1}$$

in which $e_{w,i}$ is the prewhitened EMG of muscle i, k indexes the time vector, and n is the number of samples. The mean EMG was calculated, according to

$$u_0 = \frac{1}{4}\sum_{i=1}^{4} \frac{\mathrm{IEMG}_i}{\mathrm{IEMG}_{\mathrm{ref},i}} \tag{2}$$

where $\mathrm{IEMG}_{\mathrm{ref},i}$ denotes the IEMG for muscle i of the reference condition (WB *stiff*) averaged over the four repetitions.

To calculate the muscle activation, $a(t)$, the EMG signals are scaled and expressed into Newtons. The force to EMG ratio of each muscle, K_i, is estimated from the push/pull tasks by linear regression. The (lumped) muscle activation is obtained by combining the rectified prewhitened EMGs of the four recorded muscles

$$\begin{aligned} a(t) &= \frac{1}{2}\left(K_1 |e_{w,1}(t)| + K_2 |e_{w,2}(t)|\right) \\ &\quad + \frac{1}{2}\left(K_3 |e_{w,3}(t)| + K_4 |e_{w,4}(t)|\right) \\ &= \frac{1}{2}\sum_{i=1}^{4} K_i |e_{w,i}(t)|. \end{aligned} \tag{3}$$

In this equation it is assumed that both "push" muscles (1 and 2) have equal relevance and consequently the total push force is equal to the mean of both muscles. The same holds for the "pull" muscles (3 and 4). Note that K_1 and K_2 are positive and K_3 and K_4 are negative, as the muscles operate in opposite direction.

2) Nonparametric Analysis: The time records ($x_h(t)$, $f_h(t)$, $d(t)$, and $a(t)$) of the four repetitions for one condition are averaged to reduce the variance due to noise in the signals. The signals are transformed to the frequency domain using the fast Fourier transform (FFT). Because force disturbances are applied, interaction between the subject and manipulator existed, i.e., the position of the handle depends on both the dynamics of the subject and the virtual environment imposed by the manipulator. Because of this interaction closed loop identification algorithms are required to estimate the frequency response functions (FRFs) of the mechanical admittance $\hat{H}_{fx}(f)$, and reflexive impedance $\hat{H}_{xa}(f)$ [11]

$$\hat{H}_{fx}(f) = \frac{\hat{G}_{dx}(f)}{\hat{G}_{df}(f)} \tag{4}$$

$$\hat{H}_{xa}(f) = \frac{\hat{G}_{da}(f)}{\hat{G}_{dx}(f)} \tag{5}$$

where $\hat{G}_{dx}(f)$ is the estimated cross spectral density between d and x_h (hat denotes estimate). The spectral densities are averaged over four adjacent frequencies to reduce the variance of the estimations [18]. As a measure for linearity between the signals the coherence for the position ($\hat{\gamma}_x^2(f)$) and muscle activation ($\hat{\gamma}_a^2(f)$) were estimated.

$$\hat{\gamma}_x^2(f) = \frac{\left|\hat{G}_{dx}(f)\right|^2}{\hat{G}_{dd}(f)\hat{G}_{xx}(f)} \tag{6}$$

$$\hat{\gamma}_a^2(f) = \frac{\left|\hat{G}_{da}(f)\right|^2}{\hat{G}_{dd}(f)\hat{G}_{aa}(f)}. \tag{7}$$

The coherence varies between 0 and 1 and decreases due to external noise and nonlinearities. The FRFs and coherences were only evaluated at the frequencies where the perturbation signal had non-zero power.

3) Quantification of Activation Dynamics: As described previously a secondary experiment was performed to estimate the muscle activation dynamics. During isometric experiments the relationship between the muscle activation $a(t)$ and handle force $f_h(t)$ depends on the activation dynamics only. As the muscle activation was scaled to force the muscle dynamics have unity static gain. The activation dynamics $\hat{H}_{\text{act}}(f)$ were estimated by dividing the appropriate spectral densities with the aid of an independent instrument variable [14]

$$\hat{H}_{\text{act}}(f) = \frac{\hat{G}_{wf}(f)}{\hat{G}_{wa}(f)} \tag{8}$$

$$\hat{\gamma}^2_{af}(f) = \frac{\left|\hat{G}_{af}(f)\right|^2}{\hat{G}_{aa}(f)\hat{G}_{ff}(f)} \tag{9}$$

with w as the instrument variable for which a signal with power uniformly distributed between 0.1–20 Hz was used. To improve the estimations the spectral densities are averaged over four adjacent frequencies.

The activation dynamics are parametrized by with a second-order model [19]–[21]

$$H_{\text{act}}(s, p_{\text{act}}) = \frac{1}{\frac{1}{{\omega_0}^2}s^2 + \frac{2\beta}{\omega}s + 1}$$

with

$$p_{\text{act}} = [f_0, \beta] \tag{10}$$

in which s the Laplace operator equals $j2\pi f$, f_0 is the eigenfrequency ($f_0 = \omega_0/2\pi$), β the relative damping of the activation dynamics model, and p_{act} is the parameter vector.

The activation dynamics were obtained by fitting the model (10) onto the estimated activation dynamics (8) by minimizing the criterion function:

$$L_{\text{act}}(p_{\text{act}}) = \sum_k \frac{\hat{\gamma}^2_{af}(f_k)}{1+f_k}\left|\ln \hat{H}_{\text{act}}(f_k) - \ln H_{\text{act}}(f_k, p_{\text{act}})\right|^2 \tag{11}$$

where k indexes the frequency vector. Only the frequencies to 10 Hz were used for the criterion as for higher frequencies the force signal contained little power such that the activation dynamics can not be estimated reliably. This is reflected by the low coherence for these frequencies, see Results. Because of the large range of the FRF gain a least squares criterion with logarithmic difference was used [22]. The criterion was weighted with the coherence to reduce emphasis on less reliable frequencies in the FRF and with $(1+f_k)^{-1}$ to prevent excessive emphasis on the higher frequencies. To obtain a better fit one set of parameters was used to fit the model simultaneously on all 8 trials for each subject. Finally the activation parameters were averaged over all subjects and used to quantify the intrinsic and reflexive parameters in the main experiment.

4) Quantification of Intrinsic and Reflexive Properties: The model used to quantify the proprioceptive reflexes along with the intrinsic muscle visco-elasticity and limb mass is given in Fig. 3. The position of the handle, x_h, results from (1) the external force disturbance, d, (2) human arm admittance, H_{fx}, and (3) the admittance of the virtual environment, H_e. The virtual environment is applied by the manipulator as a second-order system of which the parameters are varied between trials, see also the apparatus

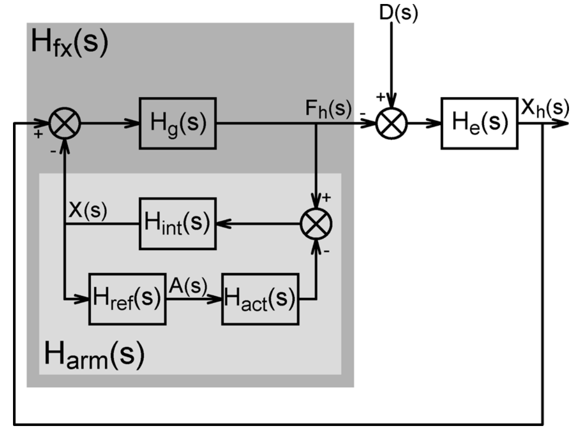

Fig. 3. NMS model $H_{fx}(s)$ in conjunction with the environment $H_e(s)$. The external force disturbance $D(s)$, hand force $F_h(s)$, position of the handle $X_h(s)$, and muscle activation $A(s)$, are measured. $H_g(s)$ represents grip dynamics, $H_{\text{int}}(s)$ intrinsic properties, $H_{\text{act}}(s)$ activation dynamics, $H_{\text{ref}}(s)$ reflexive feedback, and $X(s)$ position of the arm. The light gray box ($H_{\text{arm}}(s)$) represents the arm model without grip.

$$H_e(s) = \frac{1}{m_e s^2 + b_e s + k_e} \tag{12}$$

with $s = j2\pi f$.

The parameters of the model (gray boxes in Fig. 3) are summarized in Table I. The grip dynamics of the hand are represented by $H_g(s)$

$$H_g(s) = b_g s + k_g. \tag{13}$$

The intrinsic model, $H_{\text{int}}(s)$, includes the visco-elasticity of the co-contracted muscles and the (lumped) arm mass. For small displacements the intrinsic visco-elastic properties of muscles can be described by a linear spring-damper system [23]

$$H_{\text{int}}(s) = \frac{1}{ms^2 + bs + k}. \tag{14}$$

The reflexive dynamics, $H_{\text{ref}}(s)$, represents the muscle spindle sensory system modelled by an acceleration (k_a) velocity (k_v) and position (k_p) term in series with neural time delay, τ_d

$$H_{\text{ref}}(s) = \left(k_a s^2 + k_v s + k_p\right) e^{-\tau_d s}. \tag{15}$$

From the equations (10)–(15) the arm dynamics, excluding grip dynamics, can be derived

$$\begin{aligned} H_{\text{arm}}(s) &= \frac{X(s)}{F_h(s)} = \frac{H_{\text{int}}(s)}{1 + H_{\text{int}}(s)H_{\text{ref}}(s)H_{\text{act}}(s)} \\ &= \frac{1}{ms^2 + bs + k + \left(k_a s^2 + k_v s + k_p\right)e^{-\tau_d s}H_{\text{act}}(s)} \end{aligned} \tag{16}$$

TABLE I
MODEL PARAMETERS TO BE QUANTIFIED

m [kg]	arm mass
b [Ns/m]	muscle damping
k [N/m]	muscle stiffness
b_g [Ns/m]	grip damping
k_g [kN/m]	grip stiffness
k_a [Ns^2/m]	acceleration feedback gain
k_v [Ns/m]	velocity feedback gain
k_p [N/m]	position feedback gain
τ_d [ms]	neural time delay

where $X(s)$ and $F_h(s)$ are the Laplace transforms of the arm position and hand force respectively. Finally the mechanical admittance and the reflexive impedance are modeled by

$$H_{fx}(s,p) = \frac{X_h(s)}{F_h(s)} = H_{\mathrm{arm}}(s) + H_g^{-1}(s) \tag{17}$$

$$H_{xa}(s,p) = \frac{A(s)}{X_h(s)} = H_{\mathrm{ref}}(s)\frac{H_g(s)}{H_g(s) + H_{\mathrm{arm}}^{-1}(s)} \tag{18}$$

in which p is the parameter vector

$$p = [m, b, k, b_g, k_g, k_a, k_v, k_p, \tau_d].$$

Note that when the grip becomes very stiff, ${H_g}^{-1}(s)$ approaches to zero, such that the mechanical admittance, $H_{fx}(s)$, will become equal to $H_{\mathrm{arm}}(s)$ while the reflexive impedance, $H_{xa}(s)$, to $H_{\mathrm{ref}}(s)$.

The model parameters are quantified by fitting the models [(17) and (18)] to the corresponding FRFs [(4) and (5)] simultaneously, by minimizing the following criterion function:

$$L(p) = \sum_k \frac{\hat{\gamma}_x^2(f_k)}{1+f_k}\left|\ln \hat{H}_{fx}(f_k) - \ln H_{fx}(f_k,p)\right|^2 + q\sum_k \frac{\hat{\gamma}_a^2(f_k)}{1+f_k}\left|\ln \hat{H}_{xa}(f_k) - \ln H_{xa}(f_k,p)\right|^2 \tag{19}$$

with q as a weighting factor. Only frequencies where the perturbation signal contained power were included in the criterion. A weighting factor of 0.09 was chosen such that both terms in (19) had approximately equal values in the optimal fit.

The parameters of the conditions with WB disturbances, i.e., with and without damping and WB task *slack*, were estimated simultaneously (six conditions). During this simultaneous model fit one variable for the mass and one for the neural time delay were used for all six conditions. Except for the WB condition task *slack*, the damping and stiffness for the arm and the grip scaled between the conditions simultaneously with the mean EMG, u_0

$$\begin{aligned} b &= u_0 \cdot b_{\mathrm{ref}} \\ k &= u_0 \cdot k_{\mathrm{ref}} \\ b_g &= u_0 \cdot b_{g,\mathrm{ref}} \\ k_g &= u_0 \cdot k_{g,\mathrm{ref}} \end{aligned} \tag{20}$$

in which $_{\mathrm{ref}}$ denotes the parameter value in the reference condition. For the condition with task *slack* only the admittance was fitted ($q = 0$) and the reflexive parameters were omitted. The only function of the *slack* condition was to get a better estimate for the mass. Finally, the number of parameters was reduced from 54 (six conditions with nine parameters) to 25 (one mass, one time delay, four muscle and grip parameters for the reference condition, four idem for task *slack* and three reflex gains for five conditions).

For the NB conditions the FRFs can only be estimated for the limited bandwidth and therefore contain not enough information to estimate the nine model parameters. To overcome this, it was assumed that the intrinsic parameters (muscle and grip) scaled with mean EMG using the intrinsic parameters estimated from the reference condition (WB *stiff*), see (20). Furthermore the mass and the neural time delay were fixed to the values found with the WB conditions. Consequently the parameter vector for the NB conditions was reduced to the reflexive parameters only:

$$p = [k_a, k_v, k_p].$$

5) Model Validation: The variance accounted for (VAF) is calculated to obtain a validity index for the quantified parameters. A VAF of 100% indicates that the linear model fully predicts the measurements. Noise, nonlinearities and other unmodelled behaviour reduce the VAF. Note that a low coherence (noise or nonlinearities) always results in a low VAF values.

To calculate the VAF the model is simulated in time with the disturbance $d(t)$ as input and the simulated position $\hat{x}_h(t)$ and simulated muscle activation $\hat{a}(t)$ as the outputs. Because both the hand position and muscle activation are available from measurements, the VAF is calculated for both

$$\mathrm{VAF}_x = 1 - \frac{\sum_n |x_h(t_n) - \hat{x}_h(t_n)|^2}{\sum_n |x_h(t_n)|^2} \tag{21}$$

$$\mathrm{VAF}_a = 1 - \frac{\sum_n |a(t_n) - \hat{a}(t_n)|^2}{\sum_n |a(t_n)|^2} \tag{22}$$

in which n indexes the time sampled vector. All signals are highpass filtered to remove drift, before calculating the VAF (3th order Butterworth, 1 Hz). The lumped muscle activation signal is reconstructed from rectified EMG signals and consequently contains high frequency components. To remove these components the lumped muscle activation is lowpass filtered (third-order Butterworth, 10 Hz) before calculating the VAF.

III. RESULTS

A. Activation Dynamics

Fig. 4 shows the estimated FRFs of the activation dynamics and the coherence for a typical trial of one subject. For this trial the coherence was relatively high to 8 Hz, meaning that the estimate of the FRF is reliable to this frequency. For frequencies beyond 8 Hz the coherence dropped, which was likely the result of low input power at these frequencies. Similar figures were found for other trials and subjects. Fig. 4 also shows the fitted model for the activation dynamics for this subject. The lower plot of Fig. 4 shows the time course of the measured and predicted hand force. The predicted force resembled the recorded force very well, only at the sharp transits, i.e., higher frequencies, the force slightly deviated from the measurements. However during the main experiment these higher frequencies were

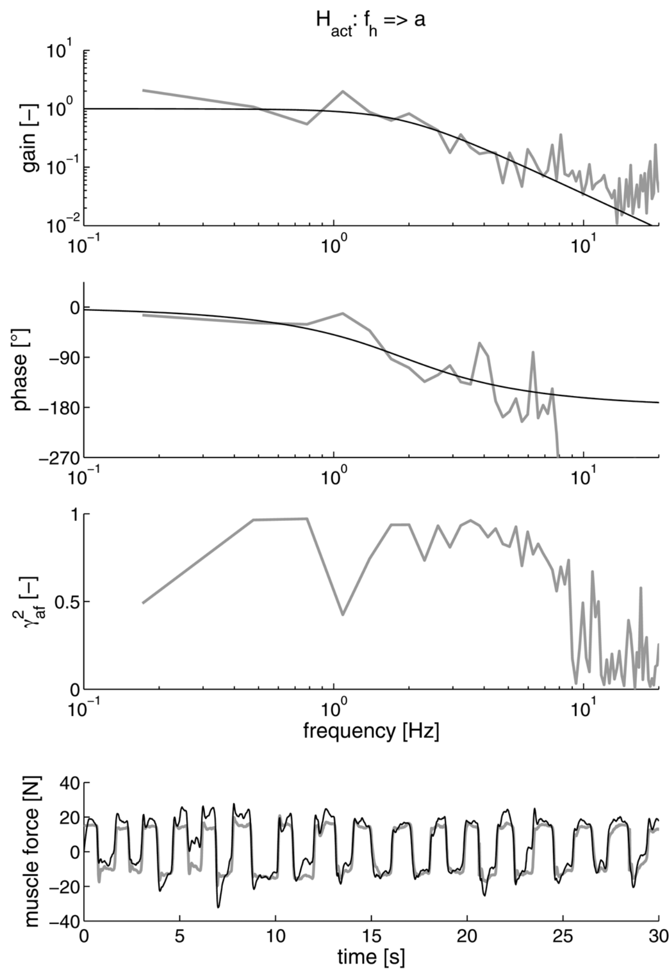

Fig. 4. From top to bottom: gain and phase of the FRF of activation dynamics, coherence, and a 10-sfragment of the recorded hand force. Black lines: model/simulation; gray lines: estimation/measurement.

TABLE II
ESTIMATED EIGENFREQUENCY, f_0, AND RELATIVE DAMPING, β, OF THE ACTIVATION DYNAMICS FOR ALL SUBJECTS

subject	f_o [Hz]	β [-]
1	1.88	0.80
2	2.58	0.77
3	2.03	0.74
4	2.00	0.74
5	2.37	0.64
mean (SD)	2.17 (0.29)	0.74 (0.06)

dominated by the arm mass and the mismatch will be of little concern.

In Table II, the estimated parameters are given for all subjects. The average values over the subjects were 2.17 Hz for the eigenfrequency and 0.74 for the relative damping. These values were used for the estimation of the intrinsic and reflexive parameters.

B. Nonparametric FRFs

In Table III the average RMS of the hand position over the subjects is given. The RMS of the hand position was always approximately 3 mm, except for NB Type 2 disturbances with center frequencies higher than 5 Hz. These disturbances only contained power above the eigenfrequency of the arm, which is approximately 3 Hz. The admittance at these frequencies was primarily determined by the arm mass, which would require uncomfortably large forces to accelerate the arm. For this reason the amplitude of the force disturbance was reduced explaining the smaller amplitudes. The mean EMG varied slightly around one, indicating that the co-activation of the muscles was almost equal for all *stiff* conditions (Table III).

TABLE III
RMS VALUE OF THE HAND POSITION AND MEAN EMG, u_0, FOR ALL CONDITIONS. MEAN (SD) OVER ALL SUBJECTS

condition		RMS [mm]	u_0 [-]
WB		3.3 (0.4)	1 (-)
B50	50 Ns/m	3.1 (0.6)	1.02 (0.05)
B100	100 Ns/m	3.1 (0.4)	0.95 (0.05)
B150	150 Ns/m	3.2 (0.5)	0.96 (0.09)
B200	200 Ns/m	3.2 (0.5)	0.93 (0.10)
NB1	1.2 Hz	3.1 (0.8)	0.95 (0.11)
NB1	1.5 Hz	3.2 (0.8)	0.94 (0.11)
NB1	1.8 Hz	3.2 (0.7)	0.95 (0.12)
NB1	2.4 Hz	3.5 (0.9)	1.01 (0.11)
NB1	3.1 Hz	3.7 (0.6)	1.01 (0.09)
NB1	3.7 Hz	3.3 (0.6)	0.99 (0.12)
NB2	1.3 Hz	3.0 (0.5)	0.98 (0.12)
NB2	1.8 Hz	2.9 (0.7)	1.05 (0.11)
NB2	2.3 Hz	3.0 (0.8)	0.99 (0.10)
NB2	3.0 Hz	2.7 (0.5)	1.03 (0.13)
NB2	4.0 Hz	3.0 (0.7)	1.06 (0.16)
NB2	5.0 Hz	2.5 (0.4)	0.95 (0.11)
NB2	6.0 Hz	2.1 (0.4)	0.97 (0.16)
NB2	7.0 Hz	1.8 (0.3)	0.98 (0.16)

Figs. 5–7 show the FRFs and coherences for one and the same subject during the WB, NB1, and NB2 conditions respectively. For all conditions the coherence of the handle position was higher than 0.95. The coherence of the muscle activation was relatively high for the frequencies between 1 and 10 Hz. With external damping the admittance decreased at low frequencies compared to the WB condition (i.e., the arm became stiffer), and the peak at the eigenfrequency around 3 Hz increased. Note that the combined arm-environment system remained well damped due to the external damping. The gain of the reflexive impedance increased with damping (upper-right plot in Fig. 5). The phase of the reflexive impedance is primarily determined by velocity feedback (differential action introducing 90 degrees phase advance at all frequencies), position feedback (zero degrees for all frequencies) and a time delay (zero phase lag at 0 Hz and increasing lag with higher frequencies). With the reference condition (WB *stiff*) the phase advance at 0.5 Hz was approximately 70 degrees, indicating that at these frequencies velocity feedback was substantial. With the increase of the external damping the phase advance at 0.5 Hz decreased, indicating that position feedback was more pronounced.

For NB1 conditions the admittance decreased with decreasing disturbance bandwidth (see Fig. 6). The peak around the eigenfrequency was not visible since the eigenfrequency was not excited by the NB1 disturbances. The reflexive impedance increased for smaller disturbance bandwidth and was almost three times larger for the smallest bandwidth compared to the reference condition.

For all NB2 conditions the gain of the admittance was lower compared to the reference condition (Fig. 7). However the reflexive impedance was increased for center frequencies up to 3 Hz, and smaller for higher center frequencies. The phase lead

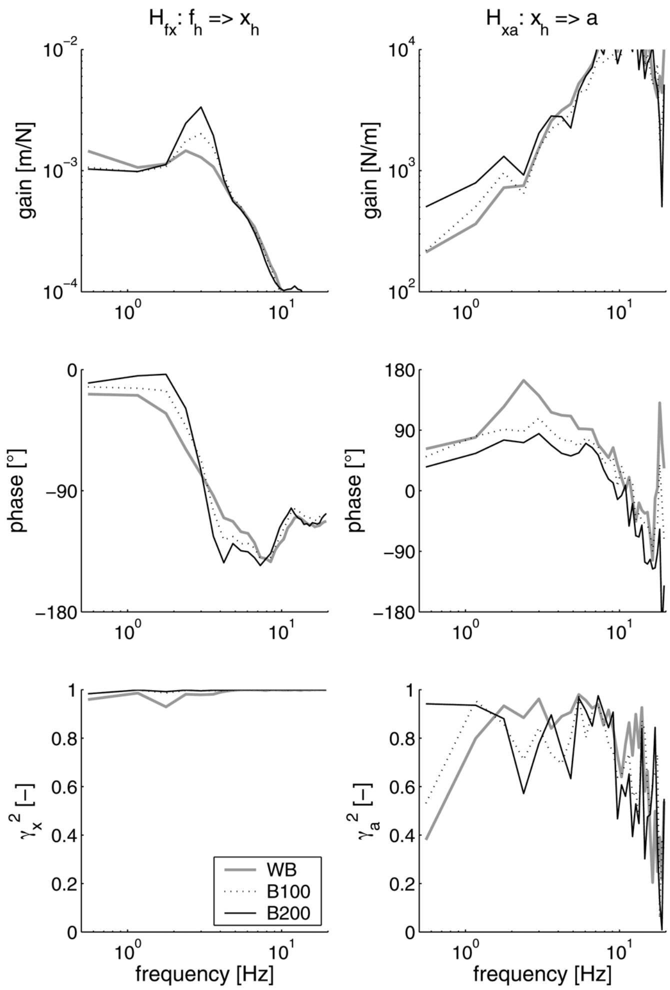

Fig. 5. FRFs of a typical subject for the mechanical admittance (left) and the reflexive impedance (right) together with corresponding coherences for WB disturbances with increasing damping. Upper row: gain; middle row: phase; bottom row: coherences.

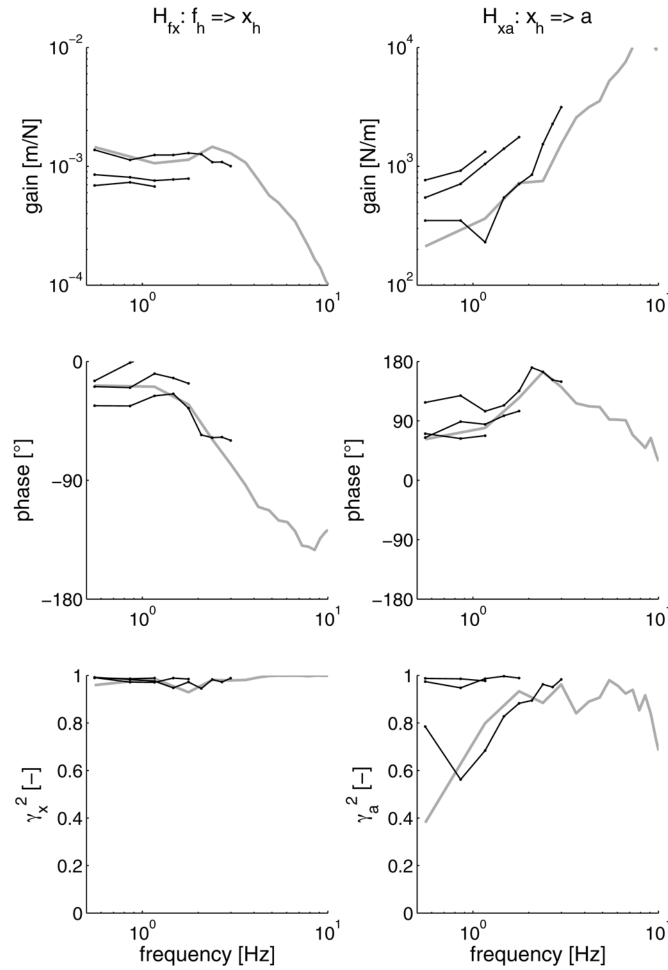

Fig. 6. FRFs of a typical subject for the mechanical admittance (left) and the reflexive impedance (right) together with corresponding coherences for NB1 disturbances. Upper row: gain; middle row: phase; bottom row: coherences. The power of the disturbances is concentrated in a small bandwidth denoted with the black lines. The gray line denotes the reference condition.

of the reflexive impedance was larger compared to the reference condition at nearly all frequencies.

C. *Intrinsic and Reflexive Parameters*

In Fig. 8 the model fit is shown for a typical subject during the reference condition. In Table IV the estimated parameters for the reference condition are given, together with the parameters for the condition with task *slack*. Fig. 9 shows the quantified parameters averaged over all subjects for all conditions together with the VAF values for position and muscle activation. The values for VAF_x (solid lines in Fig. 9) were generally high, i.e., higher than 90%. Only for the NB1 conditions with f_h smaller than 2 Hz the VAF_x was slightly smaller. The values for VAF_a varied around 50% for most conditions. Both the coherence and the VAF for the muscle activation were smaller than one, most likely due to the presence of noise in the EMG recordings. To severely reduce the noise in the signals all irrelevant frequencies, i.e., not excited by the force disturbance, were removed from the measured position and muscle activation. Noise reduction was performed by applying FFT, setting power to zero at all irrelevant frequencies, and then inverse transformation to time domain (by inverse FFT). The VAF values for these noise-reduced signals are indicated with gray lines in Fig. 9. The usage of the noise-reduced signals increased the VAF_a to values around 60% for the damping conditions and even to 90% for the NB2 conditions. The VAF_x increased to values above 90% for all conditions.

The acceleration feedback decreased with damping from around $2\ \mathrm{Ns}^2/m$ for the reference condition to $1\ \mathrm{Ns}^2/m$ for the highest external damping. As expected from the FRFs of the reference condition, the reflexive impedance was dominated by velocity feedback, which was approximately equal to the intrinsic damping. The position feedback gain increased with external damping, while velocity feedback remained almost constant. For the condition with the highest external damping the position feedback was in the same size as the intrinsic stiffness. This implicates that for this condition approximately 50% of the overall stiffness is of reflexive origin.

For the NB1 conditions both position and velocity feedback increased with decreasing bandwidth. For the largest bandwidth the reflex gains approached to the values corresponding to the reference condition. The mean values for the acceleration feedback gains did not show a clear trend with external damping. For the smallest bandwidth the standard deviations was relatively

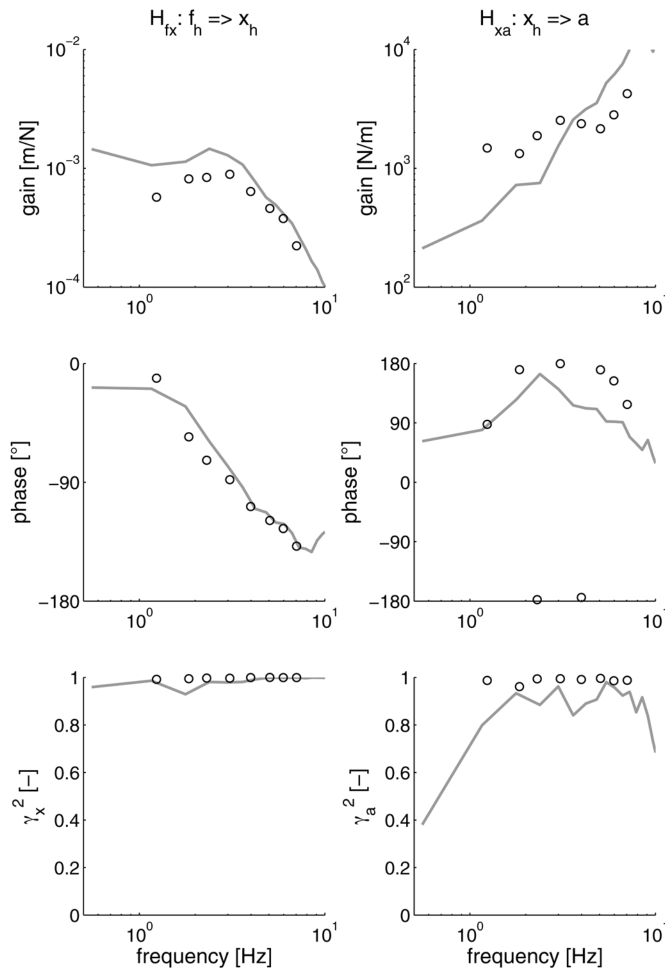

Fig. 7. FRFs of a typical subject for the mechanical admittance (left) and the reflexive impedance (right) together with corresponding coherences for NB2 disturbances. Upper row: gain; middle row: phase; bottom row: coherences. The power of the disturbances is concentrated in a small bandwidth around a center frequency denoted with the circles. The gray line denotes the reference condition.

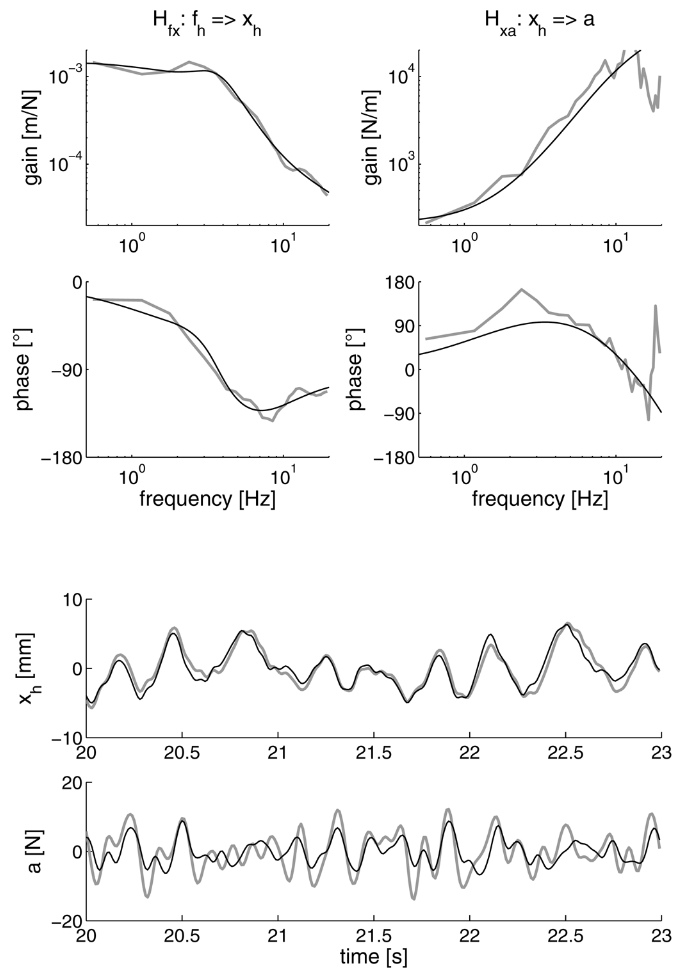

Fig. 8. Top: FRFs of the admittance (left) and reflexive impedance (right) for reference condition for a typical subject. Gray lines: estimates; black lines: model fits. Bottom: a 3 second time fragment of the handle position, $x_h(t)$, and the muscle activation, $a(t)$. Gray: measurements; black: model simulations.

high, most likely as acceleration feedback has minor effect on low frequencies.

For the NB2 conditions both the acceleration and velocity feedback increased with decreasing center frequency. The standard deviation of the position feedback is high and no trend is seen over the conditions. The high standard deviation indicates that the position feedback gain can not be quantified accurately for these conditions and has minor effect for these disturbances.

IV. Discussion

A. Methodology

In this study a method is developed to quantify the dynamic properties of proprioceptive reflexes in vivo. This method is an important tool to evaluate the regulation of proprioceptive reflexes during posture tasks. The use of force disturbances appeared natural to the subjects and facilitates the application of an unambiguous position task. Reflex gains were quantified by fitting linear models onto estimated input-output behaviour. Both the mechanical admittance and reflexive impedance were estimated on which a linear NMS model was fitted. The incorporation of the reflexive impedance into the quantification method is new and gives direct insight into the contribution of the underlying reflexive feedback system to the overall mechanical behaviour of the arm. The method has the advantage that intrinsic and reflexive parameters, including the neural time delay, can be estimated simultaneously.

The estimated coherences were high, justifying the usage of linear models. Below 1 Hz and above 10 Hz the coherence of the muscle activation was relatively low, which is likely is the result of uncorrelated corrective muscle contractions to prevent drifting of the hand position and noise inherent to EMG. The estimated FRFs of the arm admittance showed that reflexes are effective in increasing the mechanical resistance to external force disturbances, as indicated by smaller mechanical admittance and higher reflexive impedance (Figs. 5–7). The quantified parameters resulted in accurate model predictions of both hand position and muscle activation, as proved by the high VAF values for almost all experimental conditions. The small standard deviation of the estimated time delay indicates that this parameter is obtained with high accuracy. As the current method is based on Fourier analysis, the estimated delay depends on where the signals have maximum energy. This implicates that the estimated delay will be several milliseconds larger than compared with other studies, as the top in the EMG lags the EMG onset. The

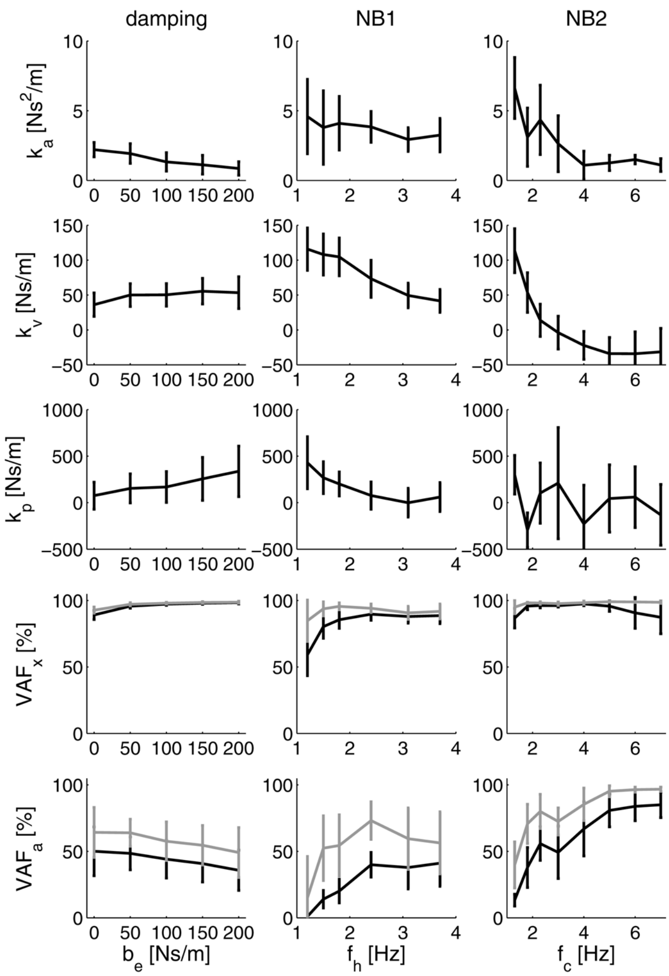

Fig. 9. Estimated reflex gains (k_a, k_v, k_p) and corresponding VAF values (VAF_x, VAF_a). Left column: external damping conditions and the reference condition ($b_e = 0\,\mathrm{NS}/m$); middle column: NB1 conditions; right column: NB2 conditions.

TABLE IV
ESTIMATED PARAMETERS FOR THE REFERENCE CONDITION AND THE CONDITION WITH TASK *SLACK*. MEAN (SD) OVER THE SUBJECTS

parameter		reference (WB *stiff*)		WB *slack*
m	[kg]	2.02 (0.39)	$\leftrightarrow$	2.02 (0.39)
b	[Ns/m]	32.5 (10.1)		14.4 (4.2)
k	[N/m]	382 (181)		169 (45)
b_g	[Ns/m]	228 (94)		44 (32)
k_g	[kN/m]	11.7 (6.0)		2.6 (1.9)
k_a	[Ns^2/m]	2.3 (0.5)		zero
k_v	[Ns/m]	37.4 (16.3)		zero
k_p	[N/m]	91 (145)		zero
τ_d	[ms]	28.4 (4.9)		-

exact lag depends on the location of the EMG electrodes over the muscle, the distance to the innervation zone and interelectrode distance. Given the mentioned effect, the mean delay of ± 29 ms indicates that the identified reflexive feedback system is mediated via monosynaptic neural connections, i.e., the short latency spinal pathways. Clear trends in the estimated reflex gains were seen which indicate that the reflex system adapts to the external condition applied. This study shows that for some condition half of the joint stiffness is of reflexive origin.

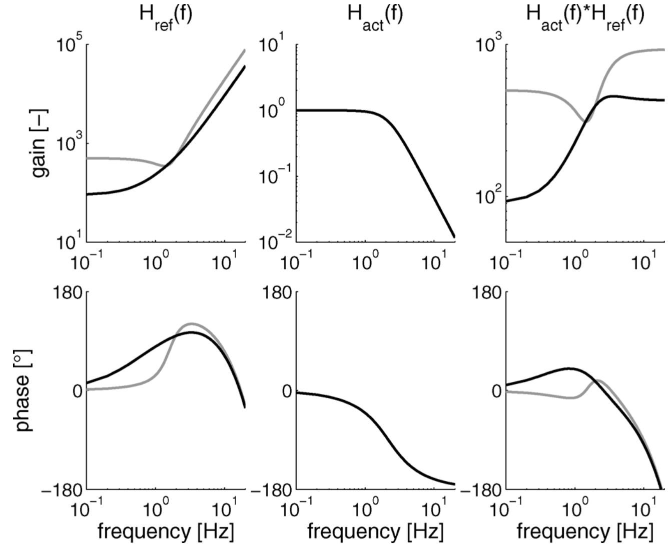

Fig. 10. Gain (upper row) and phase plots (bottom row) of the reflexive feedback $H_{\mathrm{ref}}(f)$ (left column), the activation dynamics $H_{\mathrm{act}}(f)$ (middle column) and the combined feedback controller as the cascade of both models $H_{\mathrm{act}}(f) * H_{\mathrm{ref}}(f)$ (right column). Parameter sets corresponding to the estimated values for the reference condition (black lines) and the NB1 ($f_h = 1.2$ Hz) condition (gray lines).

The values of the activation dynamics (Table II) have some variations between the subjects, especially the eigenfrequency (f_o). The average values for the activation dynamics obtained from the secondary experiment were used in the analysis of the main experiment. Setting these values constant may influence the solutions for the reflex gains. To investigate the sensitivity of the reflex gains to the dynamics of muscle activation, the eigenfrequency of the activation filter was varied by $\pm 10\%$. The effect on the reflex gains and the other parameters was small. Decreasing the eigenfrequency by 10% resulted in a shift from reflexive stiffness (k_p) to intrinsic stiffness (k) of approximately 70 N/m. Increasing the eigenfrequency by 10% had a smaller and opposite effect ($\approx$ 25 N/m). The effect on the other parameters as well as the VAF were negligable. Although a small effect was observed the trend of reflex gain variation with the loading conditions (Fig. 9) is preserved implicating that small inaccuracies in the activation dynamics will not affect the major findings of this study.

B. Functionality of Reflexes

The findings of this study add to understanding of the functionality of proprioceptive reflexes. The feedback controller is the series conjunction of muscle activation dynamics, muscle spindle dynamics and a time delay. The effect of the feedback controller is explained graphically from the feedback model shown in Fig. 10, using two different estimated parameter sets corresponding to the reference condition (black lines) and to the NB1 ($f_h = 1.2$ Hz) condition (gray lines). The muscle spindles tend to increase the feedback gain with frequency (left column) while activation dynamics causes attenuation with increasing frequency (middle column). As a result, length and velocity feedback are most effective because these properties are manifest within the bandwidth of the activation dynamics

(± 2 Hz). Beyond this bandwidth, high frequency gain from acceleration feedback (10^2 amplification per frequency decade) is cancelled due to the same amount of attenuation from the activation dynamics. Hence, the feedback system acts as a proportional-differential-proportional (PDP) controller in series with a time delay, as can be seen from Fig. 10 (right column). For the lowest frequencies the gain of the feedback system (upper right plot of Fig. 10) is proportional; for these frequencies the line is approximately horizontal. For the intermediate frequencies the slope of the line is positive, indicating a differential action. And for higher frequencies the system becomes proportional again. The effectiveness of the reflexive controller is strongly limited by substantial phase lag at higher frequencies due to the neural time delay. Attenuation of the gain at higher frequencies by the activation dynamics is therefore advantageous to facilitate position and velocity feedback, which are effective at low and intermediate frequencies. Without such an attenuation, position and velocity feedback gains would be severely limited to avoid unstable behaviour.

Besides stability as an ultimate bound, the feedback gains are determined by performance demands. High position and velocity feedback gains decrease the admittances at frequencies below the eigenfrequency of the arm (± 3 Hz), i.e., decrease the sensitivity to external force disturbance [24], [25]. However, due to the presence of phase lags from neural time delays and activation dynamics, high feedback gains also result in oscillatory behaviour around the eigenfrequency which worsen performance. In the case of the NB1 condition containing only low frequencies, the eigenfrequency is not excited and oscillations will not occur. Therefore, large feedback gains are beneficial to the performance for NB1 conditions (Fig. 10, gray lines). Furthermore, external damping suppresses the oscillation of the arm such that large feedback gains are also beneficial for these conditions (see Fig. 5). Taken together, high feedback gains improve performance at low frequencies but tend to destabilize the arm around the eigenfrequency. Apparently, the CNS modulates the feedback gains by trading off performance against stability. Future model optimisation studies could determine to what extent the quantified feedback gains found in this study are optimal.

C. Comparison With Previous Work

The experimental conditions applied in the present study were similar to those used in previous studies by our group [10], [26]. The main trends in the quantified position and velocity feedback gains are comparable, albeit that in the previous studies the velocity feedback gains were underestimated. The explanation is twofold. The first is presence of reflexive feedback during the reference condition and the second is the smaller bandwidth of the muscle activation dynamics. In the previous studies the reflexive feedback could not be identified directly and therefore it was assumed that the reflexes were negligible for wide bandwidth disturbances (reference condition) in order to separate the intrinsic and reflexive contributions. This study showed that velocity feedback was indeed present during the reference condition, hence velocity feedback was underestimated in the previous studies. In this study the activation dynamics were quantified, where in the previous studies a general model was adopted *a priori* from literature, having a bandwidth of 5 Hz. This study indicates that such a bandwidth is too high, and therefore the previously estimated velocity feedback gains were lower as a compensation.

In this study muscle activation dynamics was modelled as a second order system. The quantified cut off frequency is 2.17 Hz and the relative damping is 0.74. These values are comparable to those found in the literature. Reference [21] found a rather wide range for trunk extensor muscles (2.0–3.3 Hz) while [20] identified the elbow flexor and extensor muscles and found values of 1.9–2.8 Hz. [19] estimated values of 1.0–2.8 Hz for lower limb muscles during walking.

In this study, an acceleration term was included in the reflexive feedback to describe the reflexive impedance at higher frequencies. Reference [27] showed that linearisation of a unidirectional velocity sensitivity results in higher order terms including a pronounced acceleration term. In a recent study, the reflexive impedance was estimated from a nonlinear NMS model including unidirectional velocity sensitivity [28]. The gain and phase characteristics were comparable to those found in this study (Figs. 5–7) showing a clear second order (acceleration) response. This suggests that acceleration feedback is an artefact of muscle spindle unidirectionality rather than a distinct sensory function.

REFERENCES

[1] M. M. Mirbagheri, H. Barbeau, M. Ladouceur, and R. E. Kearney, "Intrinsic and reflex stiffness in normal and spastic, spinal cord injured subjects," *Experiment. Brain Research*, vol. 141, pp. 446–459, 2001.

[2] A. C. Schouten, W. J. T. Van de Beek, J. J. Van Hilten, and F. C. T. Van der Helm, "Proprioceptive reflexes in patients with reflex sympathetic dystrophy," *Experiment. Brain Res.*, vol. 151, pp. 1–8, 2003.

[3] R. G. Lee and W. G. Tatton, "Motor responses to sudden limb displacements in primates with specific cns lesions and in human patients with motor system disorders," *Can. J. Neurol. Sci.*, vol. 2, pp. 285–93, 1975.

[4] F. Doemges and P. M. H. Rack, "Changes in the stretch reflex of the human 1st dorsal interosseous muscle during different tasks," *J. Physiol. London*, vol. 447, pp. 563–573, 1992.

[5] F. Doemges and P. M. H. Rack, "Task-dependent changes in the response of human wrist joints to mechanical disturbance," *J. Physiol. London*, vol. 447, pp. 575–585, 1992.

[6] K. Akazawa, T. E. Milner, and R. B. Stein, "Modulation of reflex emg and stiffness in response to stretch of human finger muscle," *J. Neurophysiol.*, vol. 49, pp. 16–27, 1983.

[7] K. Kanosue, K. Akazawa, and K. Fujii, "Modulation of reflex activity of motor units in response to stretch of a human finger muscle," *Jap. J. Physiol.*, vol. 33, pp. 995–1009, 1983.

[8] L. Q. Zhang and W. Z. Rymer, "Simultaneous and nonlinear identification of mechanical and reflex properties of human elbow joint muscles," *IEEE Trans. Biomed. Eng.*, vol. 44, no. 12, pp. 1192–1209, Dec. 1997.

[9] R. E. Kearney, R. B. Stein, and L. Parameswaran, "Identification of intrinsic and reflex contributions to human ankle stiffness dynamics," *IEEE Trans. Biomed. Eng.*, vol. 44, no. 6, pp. 493–504, Jun. 1997.

[10] F. C. T. van der Helm, A. C. Schouten, E. de Vlugt, and G. G. Brouwn, "Identification of intrinsic and reflexive components of human arm dynamics during postural control," *J. Neurosci. Meth.*, vol. 119, pp. 1–14, 2002.

[11] A. Schouten, E. de Vlugt, and F. van der Helm, "Design of perturbation signals for the estimation of proprioceptive reflexes," *IEEE Trans. Biomed. Eng.*, accepted for publication.

[12] J. Ruitenbeek and R. Janssen, "Computer-controlled manipulator/display system for human-movement studies," *Med. Biol. Eng. Comput.*, vol. 22, pp. 304–8, 1984.

[13] J. Schoukens, P. Guillaume, and R. Pintelon, *Design of Broadband Excitation Signals*, K. Godfrey, Ed. Englewood Cliffs, NJ: Prentice-Hall, 1993.

[14] R. Pintelon and J. Schoukens, *System Identification: A Frequency Domain Approach*. New York: IEEE Press, 2001.

[15] E. de Vlugt, A. C. Schouten, and F. C. T. van der Helm, "Closed-loop multivariable system identification for the characterization of the dynamic arm compliance using continuous force disturbances: A model study," *J. Neurosci. Meth.*, vol. 122, pp. 123–140, 2003.
[16] E. A. Clancy, E. L. Morin, and R. Merletti, "Sampling, noise-reduction and amplitude estimation issues in surface electromyography," *J. Electromyogr. Kinesiol.*, vol. 12, pp. 1–16, 2002.
[17] G. C. Agarwal and G. L. Gottlieb, "Compliance of the human ankle joint," *J. Biomechan. Eng.*, vol. 99, pp. 166–170, 1977.
[18] G. Jenkins and D. Watts, *Spectral Analysis and Its Applications*. San Fransico, CA: Holden-Day, 1968.
[19] S. J. Olney and D. A. Winter, "Predictions of knee and ankle moments of force in walking from emg and kinematic data," *J. Biomech.*, vol. 18, pp. 9–20, 1985.
[20] J. Bobet and R. W. Norman, "Least-squares identification of the dynamic relation between the electromyogram and joint moment," *J. Biomech.*, vol. 23, pp. 1275–1276, 1990.
[21] J. R. Potvin, R. W. Norman, and S. M. McGill, "Mechanically corrected emg for the continuous estimation of erector spinae muscle loading during repetitive lifting," *Eur. J. Appl. Physiol. Occup. Physiol.*, vol. 74, pp. 119–132, 1996.
[22] R. Pintelon, P. Guillaume, Y. Rolain, J. Schoukens, and H. Vanhamme, "Parametric identification of transfer-functions in the frequency-domain – A survey," *IEEE Trans. Autom. Contr.*, vol. 39, no. 11, pp. 2245–2260, Nov. 1994.
[23] J. Winters, L. Stark, and A. H. Seif-Naraghi, "An analysis of the sources of musculoskeletal system impedance," *J Biomech.*, vol. 21, pp. 1011–25, 1988.
[24] E. de Vlugt, F. C. T. Van der Helm, A. C. Schouten, and G. G. Brouwn, "Analysis of the reflexive feedback control loop during posture maintenance," *Biolog. Cybern.*, vol. 84, pp. 133–141, 2001.
[25] A. C. Schouten, E. de Vlugt, F. C. T. Van der Helm, and G. G. Brouwn, "Optimal posture control of a musculo-skeletal arm model," *Biolog. Cybern.*, vol. 84, pp. 143–152, 2001.
[26] E. de Vlugt, A. C. Schouten, and F. C. T. van der Helm, "Adaptation of reflexive feedback during arm posture to different environments," *Biolog. Cybern.*, vol. 87, pp. 10–26, 2002.
[27] S. L. Kukreja, H. L. Galiana, and R. E. Kearney, "Narmax representation and identification of ankle dynamics," *IEEE Trans. Biomed. Eng.*, vol. 50, no. 1, pp. 70–81, Jan. 2003.
[28] A. Stienen, A. Schouten, J. Schuurmans, and F. van der Helm, "Analysis of reflex modulation with a biological neural network," *J. Comput. Neurosci.*, to be published.

Alfred C. Schouten received the M.Sc. and Ph.D. degrees in mechanical engineering from Delft University of Technology, Delft, The Netherlands, in 1999 and 2004, respectively.

Since 2004, he holds a Postdoctoral Position at the Delft University of Technology within TREND (Trauma Related Neuronal Dysfunction), a Dutch multidisciplinary research consortium on Complex Regional Pain Syndrome. He is Co-Founder of the Delft Laboratory for Neuromuscular Control. His research interest is the field of neuromuscular control and includes techniques to quantify the functional contribution of afferent feedback, neuromuscular modelling, haptic manipulators, and system identification.

Erwin de Vlugt received the M.Sc. and Ph.D. degrees in mechanical engineering at the Delft University of Technology (DUT), Delft, The Netherlands, in 1998 and 2004, respectively.

Since 2004, he holds a Postdoctoral position at DUT. His current research is focused on the modulation of spinal reflexes in vivo, both in the normal and pathological case. He is Co-Founder of the Delft Laboratory for Neuromuscular Control (NMC Laboratory). The NMC Lab holds several force controlled robots that are used for the quantification of the human spinal reflex system. One and multiple axes robots were built for the analysis of different joints. Other research activities are dedicated to system identification, neuromuscular modeling and haptic robotics.

J. J. (Bob) van Hilten received the medical, neurological, and scientific degrees at the Leiden University, The Netherlands.

He is a Professor in Movement Disorders at the Leiden University Medical Center, The Netherlands. He is a member of the Movement Disorders Society (MDS) and has served on several MDS committees, including the Evidence-based Medicine Task Force and Taskforce on the Development of Rating Scales for Parkinson's Disease. Currently, he is a member of the Executive Committee of the European section of the MDS and a member of the Research Committee on Parkinsonism and Related Disorders of the World Federation of Neurology. He has published over 100 scientific articles in the field of movement disorders. His research interests are focussed on clinimetrics, assessment techniques, intrathecal drug delivery, phenotyping of patients with Parkinson's disease and Complex Regional Pain Syndrome. In 2004 he was appointed scientific director of Trauma Related Neuronal Dysfunction (TREND), a Dutch multidisciplinary research consortium on Complex Regional Pain Syndrome.

Frans C. T. van der Helm received the M.Sc. degree in human movement science from VU University Amsterdam, The Netherlands, in 1985 and the Ph.D. degree in mechanical engineering from Delft University of Technology, Delft, The Netherlands, in 1991.

He is Professor in biomechatronics and biorobotics and Head of the Department of Biomechanical Engineering. He is a member of the board of the International Society of Biomechanics (ISB), and participates in the board of the Technical Group of Computer Simulation (TGCS), and the International Shoulder Group (ISG). He is one of Programme Leaders in the Delft Center on Biomedical Engineering. He is Principal Investigator in the TREND research consortium, investigating Complex Regional Pain Syndrome as a neurological disorder. He has published over 100 papers in international journals on topics as biomechanics of the upper and lower extremity, neuromuscular control, eye biomechanics, pelvic floor biomechanics, human motion control, and posture stability.